CHAPTER 4
THERMAL STABILITY OF NANOSTRUCTURED SURFACE LAYER

4.1 Introduction

In this chapter, the thermal stability of the nanostructured surface layer processed by ultrasonic shot peening is presented. The thermal stability and other features such as precipitation of hardening particles, grain growth kinetics and microstructural evolution of the nanostructured surface layer were investigated following the annealing at different temperatures from 150°C-350°C, using XRD and TEM. Samples of 10 mm diameter and 4 mm thickness were subjected to USSP for 300 seconds at a constant amplitude of 80 μm at a vibrating frequency of 20 kHz with hard steel balls of 3 mm diameter. The USSP treated disks were subjected to annealing at 150°C, 200°C, 250°C, 300°C and 350°C for the duration of 2, 5, 10, 20 and 30 minutes. The USSP caused dissolution of precipitates in the matrix, however, precipitates started reappearing at 200°C, coarsened at the higher temperatures and finally dissolved at around 350°C. The processes of recovery, recrystallization and grain growth resulting from the annealing treatment were also examined. The process of recrystallization in the surface region was found to start at the annealing temperature of 250°C and was completed at 350°C. The nanograins resulting from the USSP were thermally stable up to 250°C and grain coarsening occurred at higher temperature of 300°C, however, the grain size was $<$100 nm even after annealing at 350°C. The

high thermal stability of the nanostructure was due to pinning of the grain boundaries by fine precipitates. Quantitative evaluation of the different strengthening processes showed that there was strengthening from grain refinement as per the Hall-Petch relationship and dislocation hardening as per the Bailey-Hirsch relationship. This work was undertaken to understand the stability of the microstructure in terms of the size of the ultrafine grains of matrix and the different precipitates on exposure of the USSPed material at elevated temperature to explore the possibility of its application.

4.2 Differential Scanning Calorimetry

Differential scanning thermograms of the un-USSP and USSP treated specimens, at a heating rate of 10°C/min for the AA7075 are shown in Fig. 4.1. In the un-USSP condition there are three endothermic peaks (shown by up-triangles) and three exothermic peaks (shown by down-triangles). The first endothermic peak in the range of 80°C to 120°C shows formation of GP-zones and the first exothermic peak at 135°C represents dissolution of these GP-zone clusters. The second endothermic peak from 170°C to 230°C is for the formation of η'. The presence of doublet from 225°C to 250°C is attributed to transformation of the semi-coherent η' precipitates to incoherent η precipitates. The second exothermic peak at 260°C is for complete dissolution of the η' precipitates. The high temperature exotherm at 330°C indicates dissolution of the equilibrium η precipitates. In the case of USSP treated sample all the endothermic and exothermic peaks were observed to appear at lower temperatures as compared with that of the un-USSP condition. However, the intensity of the peaks for the USSP sample was relatively less.

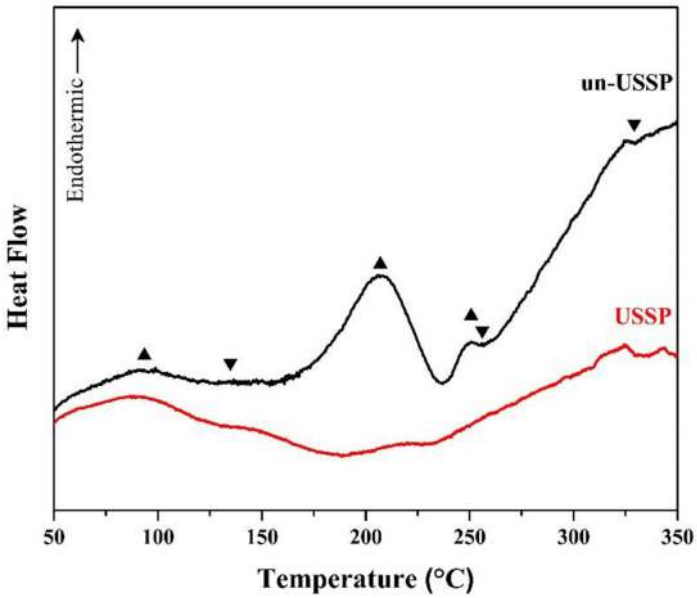

FIGURE 4.1: DSC thermograms of the AA7075 in the un-USSP and USSP treated conditions obtained at heating rate of 10°C/min.

4.3 Microhardness Variation after Thermal Exposure

The variation of microhardness of the USSP treated AA7075 in the surface region at different temperatures for the different annealing durations is shown in Fig. 4.2. For the samples annealed at the temperatures of 150°C and 200°C slight increment in hardness is observed during the initial stage of annealing, whereas it remains almost constant during the further period of annealing. On annealing at 250°C, the microhardness decreases continuously from 168 H_v with the duration of annealing and reaches to 98 H_v. Annealing at 300°C and 350°C causes rapid decrease in the hardness, initially for very short duration of annealing and remains constant with further increase in the annealing duration. The temperature of 250°C (0.56 T_m,) is seen to be transition temperature, below which the hardness remains constant and beyond it there is rapid decrease in the hardness.

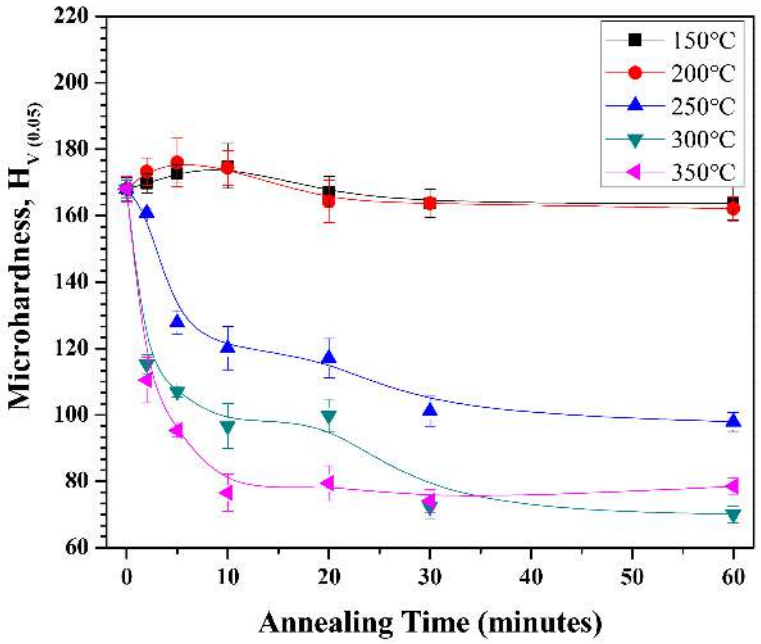

FIGURE 4.2: Variation of microhardness of the USSP treated AA7075 with the duration of annealing at different temperatures.

4.4 Phase Analysis following Annealing

The XRD patterns of the USSP treated AA7075 after annealing at different temperatures for 30 min are shown in Fig. 4.3.

Peaks of α-Al are observed along with small intensity peaks of $MgZn_2$ for the USSP treated sample. XRD pattern of the USSP treated sample annealed at 150°C is similar to that of the as USSP treated sample, however, on annealing at 200°C the intensity of $MgZn_2$ peaks increases indicating increase in volume fraction of these precipitates. The sample annealed at 250°C exhibits slightly sharper peaks of α-Al and more distinct peaks of $MgZn_2$ as compared to that annealed at 200°C. This shows that grain size of the α-Al phase increases and more $MgZn_2$ has precipitated. The peaks of both α-Al and $MgZn_2$ phase are further sharpened from annealing at 300°C indicating significant grain growth,

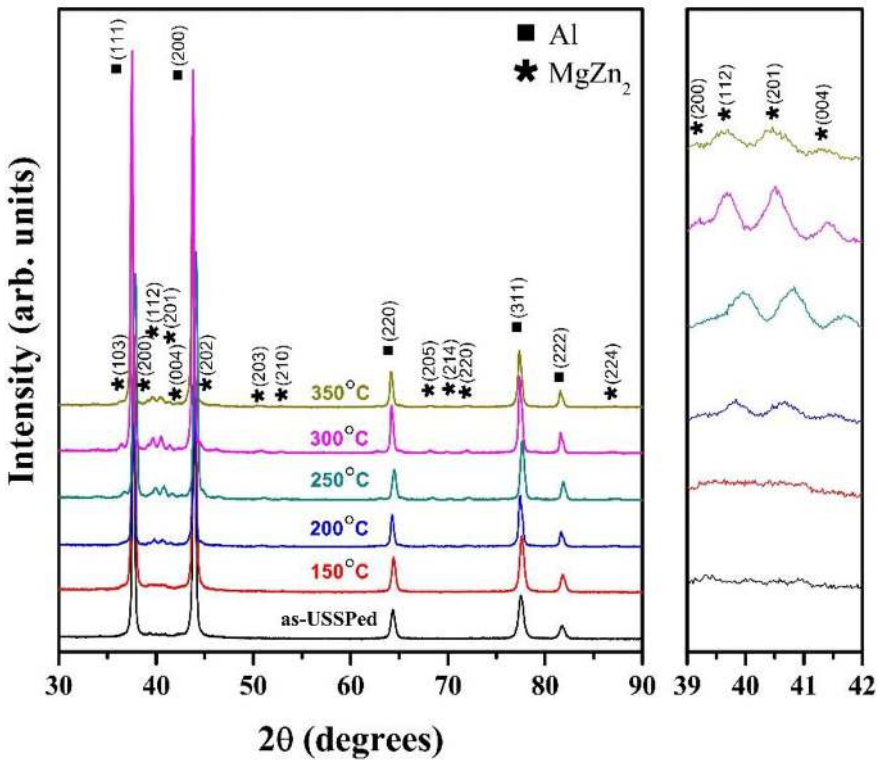

FIGURE 4.3: XRD profiles of the USSP treated sample and the USSP treated samples annealed at different temperatures for 30 minutes.

substantial increase in volume fraction of the precipitates and stress relieving. At 350°C the overall intensity of the diffraction peaks is decreased indicating dissolution of the precipitates at this temperature.

X-ray diffractograms of the USSP treated AA7075 subjected to annealing at different temperatures of 150°C, 250°C and 350°C for 2 min, 5 min, 10 min, 20 min and 30 min are shown in Fig. 4.4. The XRD pattern of the USSP treated sample annealed at 150°C is similar to that of the USSP treated sample, exhibiting diffraction peaks of Al and $MgZn_2$ with no relative change in intensity with annealing duration. At 250°C significant change is observed in the XRD pattern corresponding to $MgZn_2$. More distinct and sharper peaks of $MgZn_2$ can be observed and their intensity is increased with increase in the duration of

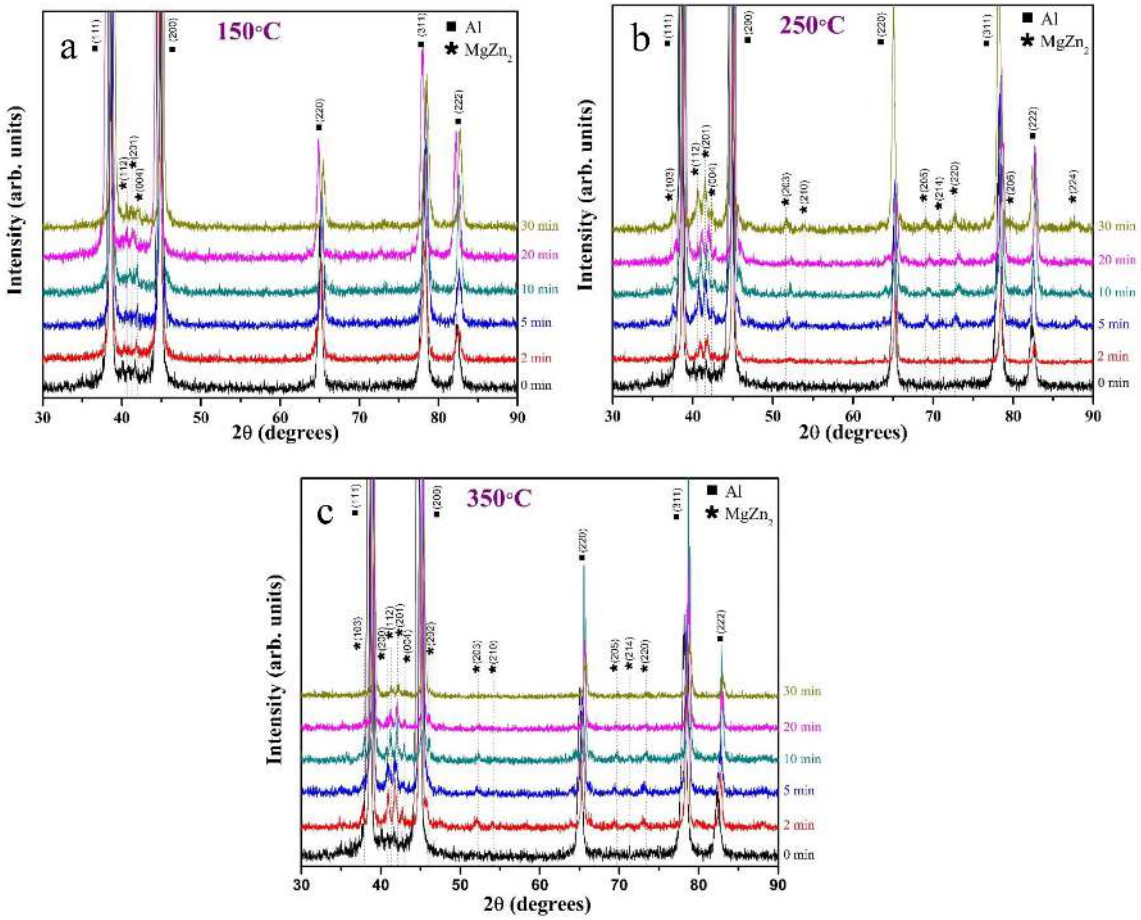

FIGURE 4.4: XRD profiles of the as USSP treated sample and the USSP treated samples following annealing at (a) 150°C, (b) 250°C and (c) 350°C for varying periods of time.

annealing and some additional reflections at higher angle, indicate more precipitation of the $MgZn_2$ phase. The peak intensity of $MgZn_2$ phase at 350°C increases sharply even at short duration of annealing for 2 min, however it decreased with increase in the duration of annealing which can be attributed to dissolution of the precipitates.

The average crystallite size for the different conditions was determined from the XRD peak broadening and is depicted in Fig. 4.5a. For the USSP treated condition, the crystallite size was 20 nm and on annealing at 150°C there was slight increase in the crystallite size and it reached to 26 nm for 30 min of annealing. Crystallite size increased

to 36 nm from annealing at 250°C for 30 min. An abrupt increase in the crystallite size was observed for even shorter duration of annealing at 350°C and the size was increased beyond the nano regime of 100 nm. The mean microstrain (Fig. 4.5b) is found to decrease continuously with increase in the duration of annealing at all the soaking temperatures of 150°C, 250°C and 350°C respectively.

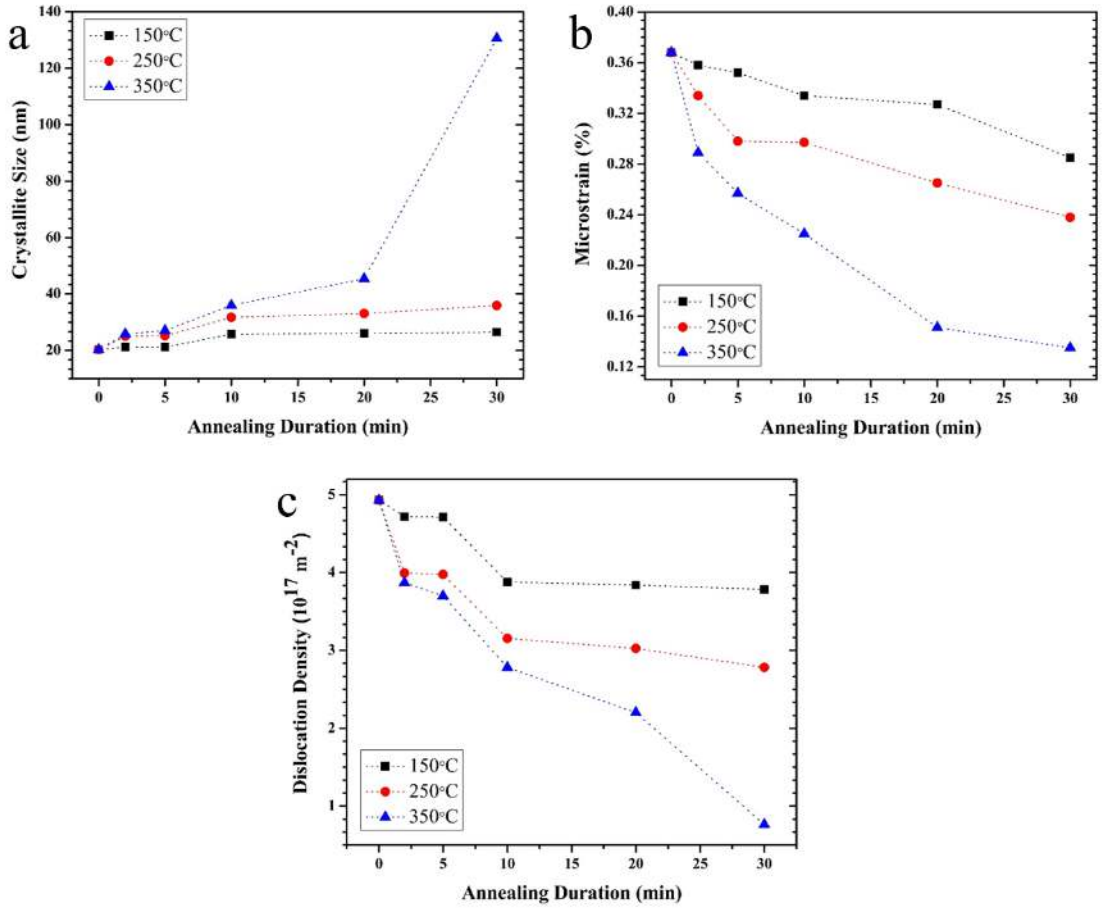

FIGURE 4.5: Variation of (a) Crystallite size, (b) Microstrain and (c) Dislocation density of the USSP treated AA7075 with duration of post annealing treatment at different temperatures.

The dislocation density ρ for the USSP treated and subsequent annealed conditions

can be represented in terms of the crystallite size D and the microstrain ϵ from the relationship [83]:

$$\rho = \frac{2\sqrt{3}\,\langle\varepsilon^2\rangle^{\frac{1}{2}}}{D * b} \tag{4.1}$$

where b is the burgers vector and equals to a/$\sqrt{2}$ for FCC structure and a is the lattice parameter. The ρ for the USSP treated sample was found to be 4.93x10^{17} m^{-2} and it decreased continuously with increase in the duration of annealing at all the temperatures of exposure (Fig. 4.5c). Annealing at 150°C for 30 min led to decrease in ρ and it reached to 3.78x10^{17} m^{-2}. Annealing at 250°C reduced the ρ further to 2.78x10^{17} m^{-2}. There was significant reduction in ρ from exposure at 350°C and it was 0.76x10^{17} m^{-2}.

4.5 Microstructural Evolution during Annealing

The microstructural changes from isothermal annealing of the USSP treated samples at different temperatures are shown in Fig. 4.6. The samples were annealed from 150°C to 350°C for constant duration of 30 min. At 150°C the original nano grained structure is retained which is evident from ring formation in the SAED pattern (Fig. 4.6a). Decrease in dislocation density is observed with increase in the subgrain size and no evidence of precipitation is noticeable. Annealing at 200°C resulted in precipitation of large amount of rod/disk shaped η ($MgZn_2$) precipitates (Fig. 4.6b). Recrystallization of the nanograins started at this temperature and majority of the blurred grain boundaries of the subgrains got converted to well defined subgrain boundaries without much change in the sub-grain size.

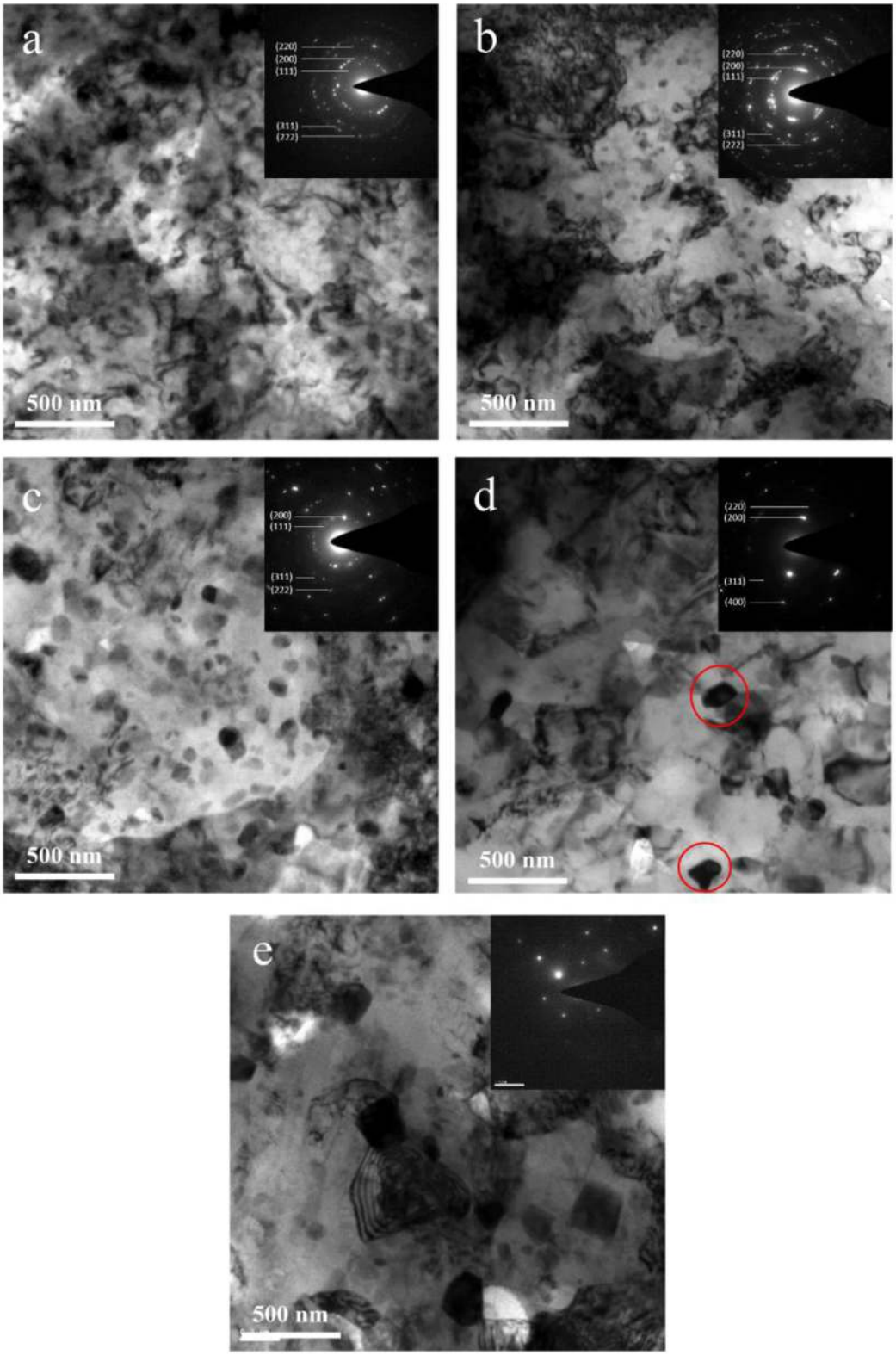

FIGURE 4.6: Bright field TEM micrographs and respective SAED patterns of the USSP treated samples annealed at (a) 150°C, (b) 200°C, (c) 250°C, (d) 300°C and (e) 350°C for 30 minutes.

With increase in the temperature to 250°C significant change was observed in the microstructure (Fig. 4.6c). The overall volume fraction and size of the precipitates were increased with simultaneous recovery of dislocations, whereas fraction of the recrystallized grains was found to increase at this temperature. At 300°C the density of the second phase precipitates further increased with coarsening of grains (Fig. 4.6d). As can be seen from the SAED pattern (inset of Fig. 4.6d), that there are streak points instead of continuous rings, indicating grain growth. Presence of some dislocation free recrystallized ultrafine grains was also observed. TEM micrograph of the sample annealed at 350°C is shown in Fig. 4.6e, such a high temperature resulted in decrease in volume fraction of the precipitates and the size of the grains was increased however, it remained at the sub micrometer level with some equiaxed recrystallized grains.

4.6 Discussion

4.6.1 Precipitation kinetics

Aluminium alloy 7075 was solution treated and subsequently quenched to dissolve the solute atoms completely in the α-Al matrix in order to have supersaturated solid solution (SSSS). The normal precipitation sequence of the AA7075 subjected to aging after solution treatment and quenching is as follows [100, 101]:

$$SSSS \rightarrow Guinier - Preston(GP)zones \rightarrow \eta'(MgZn_2) \rightarrow \eta(MgZn_2) \qquad (4.2)$$

The USSP treatment did not alter the precipitation sequence and it remained same as that of the un-USSP specimen, as revealed by the DSC result. The DSC thermograms confirm the formation of GP-zones in the temperature range of 75°C to 110°C for the USSP treated sample and they get dissolved at 125°C. These GP-zones are distributed homogeneously throughout and are fully coherent with the matrix. At around 160°C the peak of η' was observed which is also evident from the peak of the second phase precipitate in the X-ray diffractographs of the USSP treated specimen annealed at 150°C. Annealing at 200°C leads to sharp peaks of $MgZn_2$ (η') in the XRD pattern and also there was presence of a few small spherical and rod shaped precipitates in the TEM micrograph (Fig. 4.6b). The DSC curve at this temperature indicates start of transformation of η' to η precipitate and this process gets completed at around 250°C. From annealing at 250°C, a sharp increase in the intensity of XRD peak occurs for the $MgZn_2$ precipitate. The TEM micrograph shows large number of spherical particles of various sizes corresponding to $MgZn_2$ with considerable increase in their volume fraction. This result corroborates with the DSC result in which an endothermic peak is observed at 230°C due to dissolution or complete transformation of η' precipitates. Different peaks in the DSC plots for the USSP treated sample appear at lower temperature as compared to that of the un-USSP sample indicating faster precipitation kinetics. It is due to the presence of dislocations and vacancies generated during the USSP treatment which lead to faster precipitation [90]. The XRD plot shows increase in the intensity corresponding to $MgZn_2$ precipitates upto 300°C, whereas considerable drop is observed for the sample annealed at 350°C. The TEM micrograph of the 300°C annealed sample shows further reduction in volume

fraction of the precipitates whereas in the 350°C annealed sample negligible precipitates are observed. It is also evident from the DSC thermograms and the exothermic peak at 325°C that the dissolution of the η precipitates occurred.

4.6.2 Thermal stability of nanostructured surface

The thermal stability of the nanostructured surface layer of the USSP treated AA7075 was characterized by microhardness, XRD and TEM examination following annealing treatments. The variation of microhardness in Fig. 4.2 shows that there was transition in hardness value corresponding to annealing temperature of 250°C (T_t, transition temperature). Below T_t there was very little change in the hardness after prolonged duration of annealing, depicting no change in the microstructure and its thermal stability. At T_t there was gradual decrease in the hardness which may be attributed to formation of new precipitates and grain growth of the original nanograins. Beyond T_t, there occurs sharp decrease in the hardness from coarsening of grains and also due to dissolution of the strengthening precipitates at such high temperatures. These results also corroborate with the TEM observation. Similar behavior has been observed earlier also by Liu et al. [48] where they reported transition temperature of 275°C for the SMATed pure aluminium.

The microstructures of the USSP treated sample annealed at 150°C and 200°C show no significant change in the nanostructure, however, there was beginning of recrystallization at 200°C. The thermal stability of a nanocrystalline microstructure mainly depends on the grain boundary pinning by impurities (solute drag) [102, 103], pores (pore drag) [104] and second phase particles (Zener drag) [105]. The restriction to grain growth is due to the

presence of coherent precipitates, however, with increase in the annealing temperature, the density of dislocations is reduced due to annihilation and rearrangement of dislocations (Fig. 4.5d) and the grain boundaries are more clearly defined. It correlates well with the TEM observation where less dislocations are observed for the samples annealed at 200°C as compared to that annealed at 150°C. It is evident from the variation of crystallite size in Fig. 4.5a that the grain size remained almost constant from annealing at 150°C and it is also supported by the TEM micrographs in Fig. 4.6a & Fig. 4.6b. In the USSP treated sample the nanograins do not contain multiple domains, therefore crystallite size can be considered as the grain size [48]. Zhao et al. [47] reported that for the AA7075, GP zones transformed to η' at 140°C and these were stable upto 205°C. The η' precipitates being semi-coherent with the matrix restrict the mobility of the grain boundaries and thus the grain growth.

The recrystallization process somewhat increases the grain size at 250°C but the grain size still remains in the nano regime. Along with some η'-phase (plate shaped) there is also presence of η-phase (rod shaped) as some of the η' might have transformed to η. At 300°C grain coarsening took place and also there was no evidence of η'-phase. For ECAPed AA7075 it is reported that between 228°C-300°C all the η'-phase gets transformed in to η-phase [47]. As η-phase is incoherent with the matrix it barely had any effect on the grain growth thus there was coarsening of the grains. At 350°C grains were coarsened beyond the nano regime and there was formation of fully recrystallized grains and also the size of the precipitates was increased. Panigrahi et al. [106] also studied thermal stability of cryorolled AA7075 and found that submicron sized grains were stable

upto 350°C. It was due to pinning effect of fine precipitates at the grain boundaries that retarded migration of the grain boundaries. Nikitina et al. [107] studied thermal stability of the Al-Cu alloy processed by HPT (High pressure torsion) and reported grain growth beyond 200°C. Dhal et al. [108] reported ultrafine structure processed by cryo rolling to be thermally stable up to 350°C, therefore, it is also the processing route which affects the thermal stability of the alloy. Presence of large number of dislocations results in highly stable microstructure and these dislocations provide active sites for nucleation of precipitates during annealing of the USSP treated specimen. The volume fraction of precipitates increased rapidly with reduction of grain boundary area during grain growth. Due to this, the concentration of second phase particles increases along the grain boundaries resulting in stronger pinning force and hence restriction of grain boundary movement and arrest of the process of grain growth. Therefore, in the present investigation due to higher dislocation density as compared to the other SPD techniques, there was more precipitation, which helped in retention of the original nanograined structure to very high temperature.

4.6.3 Activation energy for grain growth

Grain growth in polycrystalline materials is exothermic in nature and is assisted by atomic diffusion in the grain boundary. The effect of isothermal annealing on grain growth kinetics of USSP treated AA7075 is investigated. Grain growth is expressed by the empirical formula given below [109, 110]

$$D^{1/n} - D_0^{1/n} = kt \tag{4.3}$$

Where D is the grain size at time t, D_0 is the initial grain size, k is the temperature dependent rate constant and n is the grain growth exponent. The kinetics of isothermal grain growth was obtained by fitting the data to Eq. (4.3) and the values of n is found to be 0.09, 0.143 and 0.254 corresponding to annealing temperatures of 150, 250 and 350°C respectively. The large difference in grain growth rate at low and high temperature reveals different growth regimes. At low annealing temperature of 150°C ($T \leq T_t$) it is the energy required for full recrystallization of the unrecrystallized microstructure, and at higher annealing temperature of 350°C ($T \geq T_t$) it is for the coarsening of the original nanostructured microstructure [111]. The ideal value of n is 0.5 and it is found in high-purity materials or at high annealing temperatures [112]. The difference in the value of n from 0.5 is attributed to grain boundary pinning forces which hindered the grain growth in nanostructured alloy [113].

The grain growth kinetics of USSP treated AA7075 was determined by using Arrhenius type equation

$$k = k_0 exp(-Q/RT) \tag{4.4}$$

Where k_0 is a temperature and time independent constant, R is the ideal gas constant, T is temperature of the material and Q is the activation energy for grain growth. To deduce the value of Q, average value of n (0.162) was used in the Eq. (4.4).

As shown in Fig. 4.7 the activation energy for grain growth of the USSP treated AA7075 was found to be 37.9 kJ/mol. The activation energy required for the evolution of fully recrystallized microstructure is found to be much lower than the self-lattice-diffusion

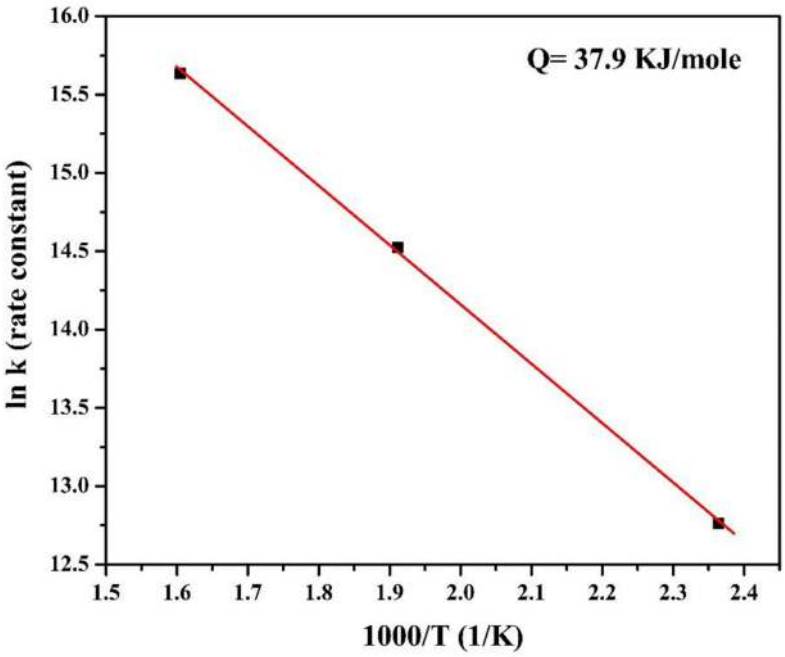

FIGURE 4.7: Plot of ln k vs 1000/T for the estimation of activation energy for grain growth of the USSP treated AA7075.

energy of polycrystalline aluminum (140.34 kJ/mol) [45] and for grain boundary self-diffusion (84 kJ/mol) [114]. The activation energy in the present case is almost equal to that of the AA6061 fabricated by accumulative roll bonding (39.2 kJ/mol) [115]. It is reported that activation energy of the Al-Mg alloy subjected to ECAP lies around 30 kJ/mol. The activation energy of USSP treated AA7075 is found to be still higher than that of the AA5083 (25 kJ/mol) processed by cryo milling [116] and to those of AA1070 (11.36 kJ/mol), AA5083 (25.10 kJ/mol) and AA2014 (20.72 kJ/mol) processed by cryo-rolling [111]. Moreover, two grain-growth regimes were observed in the nanocrystalline Al, processed by cryogenic mechanical milling within the temperature of 230–550°C and the activation energy was found to be 79 kJ/mol [45]. Other factors like grain boundary segregation, solute (impurity) drag, second phase (Zener) drag and thickness effect also

greatly affect the grain growth kinetics [48]. In the case of age-hardenable aluminium alloys presence of coherent and semi-coherent precipitates obstructs the dislocation movement during annealing, due to which the reduction in internal energy is delayed, therefore large amount of energy is absorbed in the growth of precipitates. On the other hand the pinning force exerted at the grain boundary by the precipitates inhibits the migration of grain boundary and thus retains the microstructure in the ultrafine regime annealing even at 350°C [108].

4.6.4 Mutimechanistic model of resulting hardness

In the present investigation, the microstructural changes in the USSP treated and post USSP annealed samples lead to changes in strength and hardness of the AA7075. Several strengthening mechanisms are active simultaneously in an alloy and the total hardness ΔHV_{total} constitutes of grain boundary hardening ΔHV_{GB}, solid solution hardening ΔHV_{SS}, dislocation hardening (strain hardening) ΔHV_{d} and precipitate hardening ΔHV_{p}. Therefore, the total hardness can be expressed as [117]:

$$\Delta HV_{total} = HV_0 + \Delta HV_{GB} + \Delta HV_{SS} + \Delta HV_d + \Delta HV_p \tag{4.5}$$

where, HV_0 is the hardness of annealed aluminium of 99.99% purity and is taken as ~ 20 H_v [118]. For the correlation of yield strength with hardness, σ_y was taken as 2.9 (H_v), where the unit of H_v is in MPa [119]. Quantitative evaluation of each contributing factor to the total hardness is described below and the values are depicted in the Table 4.1.

TABLE 4.1: Contribution of different hardening parameters on microhardness (H_v) of the AA7075 processed by USSP and subsequently annealed at different temperatures.

	USSP	**USSP-150°C**	**USSP-200°C**	**USSP-250°C**	**USSP-300°C**	**USSP-350°C**
Δ HV$_{grainboundary}$	90	84	77	69	55	32
Δ HV$_{solid-solution}$	12	12	12	11	10	7
Δ HV$_{dislocation}$	41	38	28	23	19	13
Δ HV$_{precipitate}$	-	-	23	16	10	10
Δ HV$_0$	20	20	20	20	20	20
Δ HV$_{Total}$	163	154	160	139	114	82
Δ HV$_{measured}$	168	164	162	98	70	78

4.6.4.1 Grain-boundary hardening

The grain-boundary hardening is usually described by the Hall-Petch relationship [120, 121]:

$$\sigma_y = \sigma_0 + k_y/\sqrt{d} \tag{4.6}$$

where σ_y is the Hall-Petch strength, σ_0 is the friction stress, k$_y$ is the Hall-Petch slope (0.12 MPa/$\sqrt{m}$ for AA7075 [122]) and d is the average grain size. Non-equilibrium grain boundaries generated during USSP treatment get eliminated on annealing of the USSP treated samples at elevated temperatures. Several studies have reported similar kind of observations in the microstructure and have applied the relationship $\Delta\sigma$=kd$^{-1/2}$ to evaluate the grain boundary strengthening [123, 124]. Therefore, in the present investigation σ_0 was not considered and the increase in grain boundary strength was considered directly proportional to d$^{-1/2}$. Considering the average grain size of 20 nm for the USSP treated specimen and 26 nm, 30 nm, 36 nm, 51 nm and 131 nm for the USSP treated samples annealed at 150°C, 200°C, 250°C, 300°C and 350°C, respectively, the values for grain boundary hardening ΔHV$_{grainboundary}$ are summarized in Table 4.1.

4.6.4.2 Solid-solution hardening

Solid-solution strengthening depends mainly on the concentration of solute atoms and is generally governed by the Fleischer model [125]:

$$\Delta\sigma_{ss} = MGb\epsilon_{ss}^{(3/2)}\sqrt{c} \tag{4.7}$$

where $\Delta\sigma_{ss}$ is the increase in strength due to solid solution hardening, M is the mean orientation factor (3.06 for FCC polycrystalline material [122]), G is the shear modulus (26.9 GPa for AA7075 [122]), b is the magnitude of Burgers vector (0.286 for FCC materials [126, 127]), ϵ is the lattice strain and c is the atomic fraction of solute atoms (0.0519 in this investigation, considering only Zn, Mg and Cu solute atoms). Local strain fields are created due to the difference in the size of solute and solvent atoms. Zn, Mg and Cu are present in the form of second phase particles in AA7075 therefore; here it is assumed that all the solute atoms are in the solid solution. Solid-solution hardening ΔHV $_{solid-solution}$ accounts for the relatively very small contribution to overall strength of the USSP treated AA7075 and its value is given in Table 4.1.

4.6.4.3 Dislocation hardening

Increase in dislocation density results in increase in the yield strength by impeding their motion through mutual interaction [128, 129]. Dislocation strengthening was evaluated using the Bailey-Hirsch relationship [130]:

$$\Delta\sigma_d = \alpha' Gb\sqrt{\rho} \tag{4.8}$$

TABLE 4.2: Precipitate size and inter-precipitate spacing of the USSP treated sample annealed at different temperatures.

Condition	Precipitate size (nm)	Inter-precipitate spacing (nm)
USSP-200°C	28.13	69.67
USSP-250°C	64.97	87.62
USSP-300°C	73.21	158.55
USSP-350°C	75.96	163.59

where$\Delta\sigma_d$ is increase in strength due to dislocation hardening, α'=0.2 for FCC metals and ρ is the dislocation density. The dislocation density used here was calculated using XRD profile refinement (Fig. 5d). The hardness contribution by dislocation $\Delta HV_{dislocation}$ is shown in the Table 4.1.

4.6.4.4 Precipitation hardening

To determine the precipitation hardening based on the Orowan looping mechanism the following Orowan equation was used [129]:

$$\Delta\sigma_{ppt} = M\frac{0.4Gb}{\pi\sqrt{1-v}}\frac{ln(2\bar{r}/b)}{\lambda_p} \tag{4.9}$$

where v is the Poisson's ratio (0.33 for AA7075 [124]), $\bar{r}$ is the mean radius of a circular cross-section in a random plane for a spherical precipitate, $\bar{r}$=$\sqrt{2}$/3r, r is the mean radius of the precipitate, λ_p is the edge-to-edge inter-precipitate spacing. The precipitates were not observed for the USSP and the sample annealed at 150°C, but precipitates were detected in the specimens annealed at higher temperatures. The mean radius of the precipitates and the mean edge-to-edge inter-precipitate spacings are given in the Table 4.2 and the values of precipitation hardening $\Delta HV_{precipitate}$ are shown in Table 4.1.

4.6.4.5 Total hardening

The total hardening factor ΔHV_{Total} calculated by adding the values from the different hardening mechanisms is almost comparable to that of the measured hardness values ($\Delta HV_{measured}$) for the USSP and the other specimens annealed at different temperatures. Some deviation was observed in the calculated hardness from the measured value of the 250°C and 300°C annealed samples which might be due to some other microstructural changes rather than the parameters used in the above calculations. When the USSP treated samples were annealed above 200°C there was decrease in the hardness. During annealing there was decrease in dislocation density due to recovery and grain growth occurred due to which nanostructure is not retained. Also decrease in solute concentration occurs due to precipitation [124]. Thus, decrease in the values of ΔHV_d, ΔHV_{gb} and ΔHV_{SS} is observed. Precipitation hardening is dependent on r and λ_p and is independent of crystal structure and chemical composition of the precipitates. It is directly proportional to number density of the precipitates. Due to the challenges in identifying the chemical composition and crystal structures of the precipitates, the Orowan dislocation bypassing mechanism was found to be the operative strengthening mechanism. Some investigators have reported grain boundary hardening as the major contributor in strengthening [131], whereas some have also reported dislocation hardening [127, 132] and precipitation hardening [122] as the main contributing factors to strengthening. In the present investigation grain-boundary hardening and dislocation hardening mechanisms are found to be governing factor for the increase in hardness of the USSP treated samples and the contribution of solid solution hardening and precipitate hardening was relatively less. Thus, using the

different strengthening equations the comprehensive comparison of the calculated and experimentally measured hardness for the USSP treated AA7075 and after its subsequent annealing can be validated. The quantitative understanding of the relationship between the microstructure and the hardness provides a basis for designing advanced high performance nanostructured materials.

4.7 Conclusions

The following conclusions are drawn from this chapter:

1. A nanostructured layer with average grain size of $\sim$ 25 nm was generated by USSP treatment of the peak aged AA7075.

2. The USSP process accelerated the precipitation kinetics but did not change the sequence of precipitation.

3. Nanograins were thermally stable upto 250°C above it there was grain coarsening but still the size was in the ultrafine regime ($<$100 nm) even after annealing at 350°C for 30 minutes.

4. The high thermal stability was due to the pinning effect of the precipitates at the grain boundaries which retarded the grain growth.

5. For the USSP treated specimen, strengthening by grain boundaries and dislocations are the dominant processes, the contribution of solid-solution strengthening and precipitate strengthening is relatively less.